Submission to ***Biofabrication*** (Article ID: BF-103870)

Low Temperature Hybrid 3D Printing of Hierarchically Porous Bone Tissue Engineering Scaffolds with *In Situ* Delivery of Osteogenic Peptide and Mesenchymal Stem Cells

Jiahui Lai[2,†], Chong Wang[1,3,†,*], Jia Liu[4,†], Shangsi Chen[2], Chaoyu Liu[5], Xiangxuan Huang[6], Jing Wu[1], Yue Pan[7], Yuancai Xie[8,*], Min Wang[2,*]

[1]School of Mechanical Engineering, Dongguan University of Technology, Dongguan, Guangdong, China

[2]Department of Mechanical Engineering, The University of Hong Kong, Pokfulam Road, Hong Kong

[3]Guangdong-Hong Kong-Macao Joint Laboratory for Neutron Scattering Science and Technology, China

[4]Department of Orthopaedics, Affiliated Hospital of Youjiang Medical University for Nationalities, Baise, Guangxi, China

[5]Department of Research and Development, Shenzhen Shiningbiotek Company Limited, Shenzhen, Guangdong, China

[6]School of Chemical Engineering and Energy Technology, Dongguan University of Technology, Dongguan, Guangdong, China

[7]Guangdong Provincial Key Laboratory of Malignant Tumor Epigenetics and Gene Regulation, Guangdong-Hong Kong Joint Laboratory for RNA Medicine, Medical Research Center, Sun Yat-Sen Memorial Hospital, Sun Yat-Sen University, Guangzhou 510120, China

[8]Department of Thoracic Surgery, Peking University Shenzhen Hospital, Shenzhen

Keywords: *Low temperature hybrid 3D printing, osteogenic peptide, hydrogel, cell delivery, tricalcium phosphate*

* Correspondence to: Dr. Wang Chong, School of Mechanical Engineering, Dongguan University of Technology, 1 Daxue Road, Songshan Lake, Dongguan, China, Email: wangchong@dgut.edu.cn; Dr. Yuancai Xie, Department of Thoracic Surgery, Peking University Shenzhen Hospital, Shenzhen, Guangdong, China, Email: xieyuancai2005@126.com; Prof. Min Wang at the University of Hong Kong, Hong Kong Fax: +852 2858 5415; Tel: +852 3917 7903; Email: memwang@hku.hk.

† These authors contributed equally.

ABSTRACT

Compared to other conventional scaffold fabrication techniques, 3D printing is advantageous in producing bone tissue engineering scaffolds with customized shape, tailored pore size/porosity, required mechanical properties and even desirable biomolecule delivery capability. However, for scaffolds with a large volume, it is highly difficult to get seeded cells to migrate to the central region of the scaffolds, resulting in an inhomogeneous cell distribution and therefore lowering the bone forming ability. To overcome this major obstacle, in this study, cell-laden bone tissue engineering scaffolds consisting of osteogenic peptide (OP) loaded β-tricalcium phosphate (TCP)/poly(lactic-*co*-glycolic acid) (PLGA) (OP/TCP/PLGA, designated as OTP) nanocomposite struts and rat bone marrow derived mesenchymal stem cell (rBMSC)-laden gelatin/GelMA (GG) hydrogel rods were produced through "dual-nozzle" low temperature hybrid 3D printing. The cell-laden scaffolds exhibited a bi-phasic structure and had a mechanical modulus of about 19.6 MPa, which was similar to that of human cancellous bone. OP can be released from the hybrid scaffolds in a sustained manner and achieved a cumulative release level of about 78% after 24 days. rBMSCs encapsulated in the hydrogel rods exhibited a cell viability of about 87.4% right after low temperature hybrid 3D printing and could be released from the hydrogel rods to achieve cell anchorage on the surface of adjacent OTP struts. The OP released from OTP struts enhanced rBMSCs proliferation. Compared to rBMSC-laden hybrid scaffolds without OP incorporation, the rBMSC-laden hybrid scaffolds incorporated with OP significantly up-regulated osteogenic differentiation of rBMSCs by showing a higher level of alkaline phosphatase (ALP) expression and calcium deposition. This "proof-of-concept" study has provided a facile method to form cell-laden bone tissue engineering scaffolds with not only required mechanical strength, biomimetic structure and sustained biomolecule release profile but also excellent cell delivery capability with uniform cell distribution, which can improve the bone forming ability in the body.

INTRODUCTION

Bone tissue engineering becomes a popular strategy to produce biological substitutes to restore, maintain or improve bone tissue function. Classic bone tissue engineering requires biodegradable, biocompatible three-dimensional (3D) scaffolds, chemical cues/biomolecules, and seed cells to achieve improved bone regeneration. It is known that 3D scaffolds are very important as they serve as extracellular matrix (ECM)-like platform to provide cells with mechanical support, facilitate their attachment and act as template for new bone tissue formation[1, 2]. Bioactive agents such as calcium phosphates and biologically active biomolecules such as bone morphogenetic protein-2 (BMP-2) [3-5] and osteogenic peptide (OP) [6] can be loaded into/onto scaffolds to provide osteoconductivity and osteoinductivity, eliciting desirable cellular responses from seed cells such as osteoprogenitors and mesenchymal stem cells (MSCs) for accelerated bone regeneration. Comparing to dense bone repair biomaterials, porous bone tissue engineering scaffolds mimicking the natural bone ECM can provide better substrates for cell attachment, morphogenesis, proliferation and differentiation and have been fabricated using a variety type of techniques, such as particle/salt leaching [7], gas foaming [8], emulsion freezing/freeze drying [9], phase separation [10] and electrospinning [11]. However, these techniques have challenges in accurately controlling the architecture (porosity, pore size, interconnectivity, shape, etc.) and properties (physical and mechanical) of bone scaffolds. In recent years, 3D printing, also known as additive manufacturing, greatly improves the ability to accurately fabricate complex scaffolds with designed architectures and properties through allocating biomaterials, biochemical signals and even living cells in a layer-by-layer manner [12, 13]. Bone tissue engineering scaffolds have been widely created via different 3D printing technologies such as extrusion-based printing [14], selective laser sintering (SLS) [15], 3D powder binding (3DPB) [16], and digital light projection (DLP) [17] using various biomaterials including polymers [3, 18], ceramics [16, 19-

21], metals [22] and their composites [6, 15, 23-25]. Towards the fabrication of biodegradable bone tissue engineering scaffolds, synthetic polymers are usually 3D printed into scaffolds with desirable mechanical properties, but the processing conditions are relatively harsh, hence the direct loading of biomolecules and cells in such materials is normally avoided [16, 26]. On the contrary, natural polymeric hydrogels such as sodium alginate and gelatin-methacryloyl (GelMA) are often used to load cells to fabricate cell-laden constructs, however, their weak mechanical strength restricts their further application in regenerating bone in load-bearing regions [27-30]. To avoid the drawbacks of synthetic and natural polymers, hybrid 3D printing of a synthetic polymer ink and a cell-laden natural polymer bioink has been performed to obtain cell-laden scaffolds with good mechanical support. However, there are still problems in the current hybrid 3D printing technologies. For example, Cho *et al.* used a dual-nozzle printer to fabricate mechanically strong and cell-laden constructs by melt extruding synthetic polymers (e.g., polycaprolactone (PCL), polylactic acid (PLA)) and depositing cell-laden hydrogels (e.g., collagen, alginate/gelatin) into the gap between two paralleled synthetic polymer struts [3, 31]. Although good mechanical strength can be obtained, PCL or PLA scaffolds still lacked hierarchical porous structures which are important for cell attachment and spreading. Meanwhile, if cells are blocked in such hydrogels for a long time, the cell morphogenesis would be delayed. Furthermore, since the fabrication involved high temperature during the printing process, biomolecules could only be loaded into hydrogel rods, resulting in a very quick biomolecule release and hence inability to achieve a long-term induction of mesenchymal stem cells and bone regeneration. Belleghem *et al.* alternately extruded a sodium alginate/poly(ethylene) glycol hydrogel ink and a fibroblast-laden GelMA bioink to create cell-laden constructs via a double-nozzle extrusion printer [32]. However, such a hybrid design was used for producing scaffolds to maintain the shape of soft tissue due to the relatively weak mechanical strength. In the tissue engineering field, it is still challenging to fabricate a cell-

laden bone tissue engineering scaffold with hierarchical porous structure, good mechanical strength, sustained delivery of biomolecules, from which the delivered cells can launch morphogenesis at appropriate time.

Cryogenic 3D printing is a recently developed technology that has been applied to process emulsion inks into porous tissue engineering scaffolds at a low temperature [33]. The cryogenic environment can help the extruded struts remain stable and protect the printed part from collapsing. Besides, the scaffolds printed at low temperature exhibit hierarchical porous structures with both interconnected macropores and micropores on strut surface, where the size of micropores could be controlled by adjusting the ratio of water phase and oil phase in the emulsion ink [34]. The hierarchical porous structures of the scaffolds provide desirable biomimetic structure which is similar to that of native cancellous bone. Also, the cryogenic 3D printed scaffolds made from synthetic polymers exhibit a mechanical strength at about tens of MPa which is comparable to the human cancellous bone [33-35]. Finally, osteogenic biomolecules such as BMP-2 and osteogenic peptide (OP) can be loaded into the water phase of the emulsion inks and encapsulated into the scaffolds during cryogenic 3D printing process [4, 6, 33], which is hard to be achieved by other 3D printing technologies such as SLS and FDM since they involve high temperatures during the fabrication process which causes inactivation of biomolecules. Therefore, cryogenic 3D printed scaffolds simultaneously achieve desirable biomimetic structure (i.e., hierarchically porous structure), suitable mechanical strength (i.e., comparable to human cancellous bone) and improved bone forming ability (i.e., controlled delivery of osteogenic biomolecules such as BMP-2 and OP). However, it is impossible to directly print out cell-laden bone tissue engineering scaffolds through cryogenic 3D printing solely. If cells are blended with synthetic polymer emulsion to formulate printing inks, both the organic solvent and cryogenic environment will damage cells. Therefore, post-fabrication cell seeding is still the only way to load cells in such scaffolds. However, the

post-fabrication cell seeding strategy causes inhomogeneous cell distribution in the scaffolds both at the micro scale (i.e., on the struts) and at the macro scale (i.e., different regions of the scaffold). To solve these problems once for all, developing a strategy to simultaneously load seed cells during the 3D printing of biomimetic scaffolds to achieve a uniform cell distribution is highly desirable for making cell-laden bone tissue engineering scaffolds with favorable features.

In this investigation, based on our previous research on cryogenic 3D printing, a low temperature hybrid 3D printing technology was developed to produce cell-laden bone tissue engineering scaffolds with suitable mechanical properties, hierarchical porous structure and excellent delivery capability of osteogenic biomolecules and cells, via alternately printing OP loaded β-tricalcium phosphate (TCP)/poly(lactic-*co*-lgycolic acid) (PLGA)/dichloromethane (OP/TCP/PLGA/DCM, designated as OTP/DCM) composite inks and rat bone marrow derived MSCs (rBMSCs) loaded gelatin/GelMA (GG) hydrogel bioinks, in which the cell-laden hydrogel rods were filled into the gaps of adjacent OTP struts at each layer. The hydrogel rods can protect cells from un-evaporated organic solvents in OTP struts during the printing process and cells can be released from hydrogels later to facilitate the cell migration and attachment onto the surface of OTP struts. Such design reconciled the paradox that sufficient mechanical strength, biomimetic porous structure and excellent delivery capabilities of biomolecules and cells cannot be easily obtained at the same time. The structure and morphology of the cell-laden scaffolds were examined using digital camera, fluorescence microscope and SEM. The mechanical properties of cell-scaffold constructs were obtained through compression testing. The *in vitro* release behavior of OP from the cell-laden scaffolds was investigated. The viability of rBMSCs right after 3D printing and released from hydrogels/attached the OTP struts was investigated using live and dead assay. The osteogenic differentiation and mineralization of

rBMSCs within the cell-laden constructs was examined by conducting alkaline phosphatase (ALP) assay and alizarin red S (ARS) assay, respectively.

MATERIALS AND METHODS

Materials

Poly(lactic-*co*-glycolic acid) (PLGA) with a molecular weight of 100,000 was provided by Jinan Daigang Biotechnology Limited, Jinan, China. β-TCP nanoparticles with an average diameter of less than 200 nm were supplied by Shanghai Aladdin Inc. China. Deionized (DI) water for all experiments was obtained using a DI water producer (Model D12681, Barnstead International, USA). Gelatin, methacrylic anhydride (MA), polyvinyl alcohol, phosphate buffered saline (PBS) tablets and bovine serum albumin (BSA) were Sigma-Aldrich products (USA). Dichloromethane (DCM) was supplied by Uni Chem Co. Korea. Osteogenic peptide (OP) with a sequence of KIPKA SSVPT ELSAI STLYL SGGC and a purity of 98.12% was supplied by Shanghai Ziyu Biotechnology Ltd, China. All reagents were directly used in the experiments without further purification. GelMA used in this study was synthesized based on previous literature [36, 37]. Briefly, 10 g gelatin (type A, from porcine skin) was firstly dissolved in 100 ml PBS at 50 °C. 0.8 ml MA was then added into the gelatin solution and the reaction was continued for about 3 hours. Next, the mixture was transferred to dialysis tubes and was dialyzed against DI water for one week at 40 °C. Finally, the mixture was put into one-well plates and froze at -70 °C overnight, followed by freeze-dried for 5 days and stored at -20 °C for further use. The degree of methacrylation (DoM) of synthesized GelMA was characterized using ^{1}H nuclear magnetic resonance (NMR) and the DoM was calculated to be about 20.6% (Fig. S1). The ^{1}H NMR characterization details of GelMA were described in the Supporting Information.

Preparation of OP/TCP/PLGA/DCM (OTP/DCM) water/oil emulsion inks

Typically, 2 mL of DI water was first blended with 10 mL of PLGA/DCM solution (30%, w/v), 50 μg of polyvinyl alcohol (PVA, acting as an emulsion stabilizer to contribute to the distribution of TCP particles) and 3 g of TCP particles. After 5 min of ultra-sonication, water/oil emulsion inks with uniform distribution of TCP were successfully formed, followed by the addition of 100 μL of PBS containing 10 mg of OP and 5 min of manual stirring, obtaining OTP/DCM emulsion inks for low temperature 3D printing. The water phase in the emulsion inks could protect OP from the inactivation induced by DCM.

Cell culture

rBMSCs were cultured with Dulbecco's modified Eagle's medium, (DMEM, Gibco, USA) which was supplemented with 10% fetal bovine serum (FBS, Gibco, USA), 100 U/ml penicillin-streptomycin (Gibco, USA) and maintained in a humidified incubator at 37 °C with 5% CO_2. The medium was changed every 2 days. The cells were cultured until 80-90% confluence was achieved and then cells were trypsinized and counted, and subjected to the preparation of rBMSCs-laden Gelatin/GelMA (GG) hydrogel inks.

Preparation of Gelatin/GelMA (GG) bioinks containing rBMSCs

Gelatin and GelMA hydrogels were applied for preparing the bioink containing rBMSCs. The gelatin or GelMA hydrogel has a thermo-reversible sol-gel property, showing a liquid state at 37 ºC and a gel state at a temperature lower than 20 ºC. The thermo-responsive gelatin played two roles in the bioink formulation: (1) increasing the viscosity of GelMA hydrogel without affecting its crosslinking degree to provide better extrusion stability during printing and improve the structural stability of as-extruded hydrogel rods; (2) facilitating the cell release from GG hydrogels during incubation because the unmodified gelatin could be quickly dissolved in the culture medium at 37 °C and then removed from the crosslinked GG hydrogels. Besides gelatin, GelMA was added to provide photocrosslinking ability to stabilize the

structures after printing. To prepare the bioink, 0.1 g gelatin and 0.1 g GelMA were firstly dissolved in 2 mL PBS at 50 °C, followed by addition of 5 μL (2-Hydroxy-2-methylpropiophenone) (a Sigma-Aldrich product) as the photoinitiator. The prepared GG hydrogels were not crosslinked before the sterilization and addition of living cells. The GG hydrogels were sterilized at room temperature by ^{60}Co γ-irradiation for 20 min. Making use of the thermo-reversible sol-gel transition of GG hydrogels, the sterilized and uncrosslinked GG hydrogel precursor was heated to 37 ºC and became a liquid state. 2 mL DMEM containing about 2×10^6 cells/ml was then added into the 2 mL liquid GG solution and mixed thoroughly via mild mechanical stirring. The obtained GG hydrogel precursor containing living cells was transferred to a syringe, which was stored at 4 °C for about 3 mins to let the bioink become a sol-gel state quickly for subsequent low temperature 3D hybrid printing.

Rheological characterization of printing inks

Before printing, the rheological properties of the OTP/DCM emulsion ink and GG bioink were studied using a rotational rheometer (MCR302, Anton Paar, Austria) with a 25 mm parallel plate and 0.55 mm measurement gap. Two rheological tests were performed: (1) shear viscosity test in a range of shear rate 0.01-1000 1/s at 24 °C (i.e., extrusion temperature); (2) angular frequency sweep in a range of frequency 1-100 rad/s at a constant strain of 0.5% under 24 °C. The strain for the angular frequency sweep was selected based on the linear viscoelastic region (LVR) of the samples, which was determined from the strain sweeps in a strain range of 0.1% to 100% at the frequency of 1 Hz.

Low temperature hybrid 3D printing of cell-laden scaffolds

Following a protocol in our previous studies, OP/TCP/PLGA scaffolds and TCP/PLGA scaffolds (designated as OTP and TP, respectively) with pre-designed structures can be produced via the low temperature 3D printing, in which the temperature of the printing

substrate was set as 5 ˚C [6, 33, 34]. For producing cell-laden composite scaffolds comprising of rBMSCs-laden GG hydrogel rods and OTP struts (designated as "GGOTP"), a dual-nozzle 3D printer (R-GEN200, regenHU Ltd, Switzerland) was used to perform the simultaneous deposition of OTP struts and rBMSCs-laden GG rods alternately in a low temperature environment, as illustrated in Fig. 1. During the low temperature hybrid 3D printing, the OTP ink was filled into syringe 1 and the rBMSCs-laden GG bioink was filled into syringe 2. The temperature of two syringes can be controlled separately. The printing parameters for the OTP ink were set as: pneumatic pressure (2.2-2.5 bar), printing speed (10 mm/s), layer thickness (0.2 mm), nozzle inner diameter (0.41 mm, 22 G); while those for the rBMSCs-laden GG bioink were set as: piston speed (0.031 mm/s), printing speed (12 mm/s), syringe temperature (24 °C), layer thickness (0.2 mm), nozzle inner diameter (0.26 mm, 25 G). The temperature of the printing substrate was set as 5 ºC. After printing one layer of OTP struts, the printer was suspended to wait for the drying of the OTP struts and then continued to deposit the rBMSCs-laden GG rods among the gaps of the OTP struts. During the suspension of the 3D printer, nearly all DCM in the OTP struts was evaporated, and hence the damage of traced DCM to the cells encapsulated in the GG rods was mitigated. With the removal of DCM, the OTP could be solidified and able to support the printed part. The 3D printing process was repeated to fabricate final 3D cell-laden scaffolds, which were then subjected to an UV irradiation at 365 mW for 30 s to crosslink the cell-laden GG hydrogel rods in scaffolds. Besides, cell-laden TP (i.e., GGTP) scaffolds were also produced as a control for evaluating the cell growth and osteogenic differentiation.

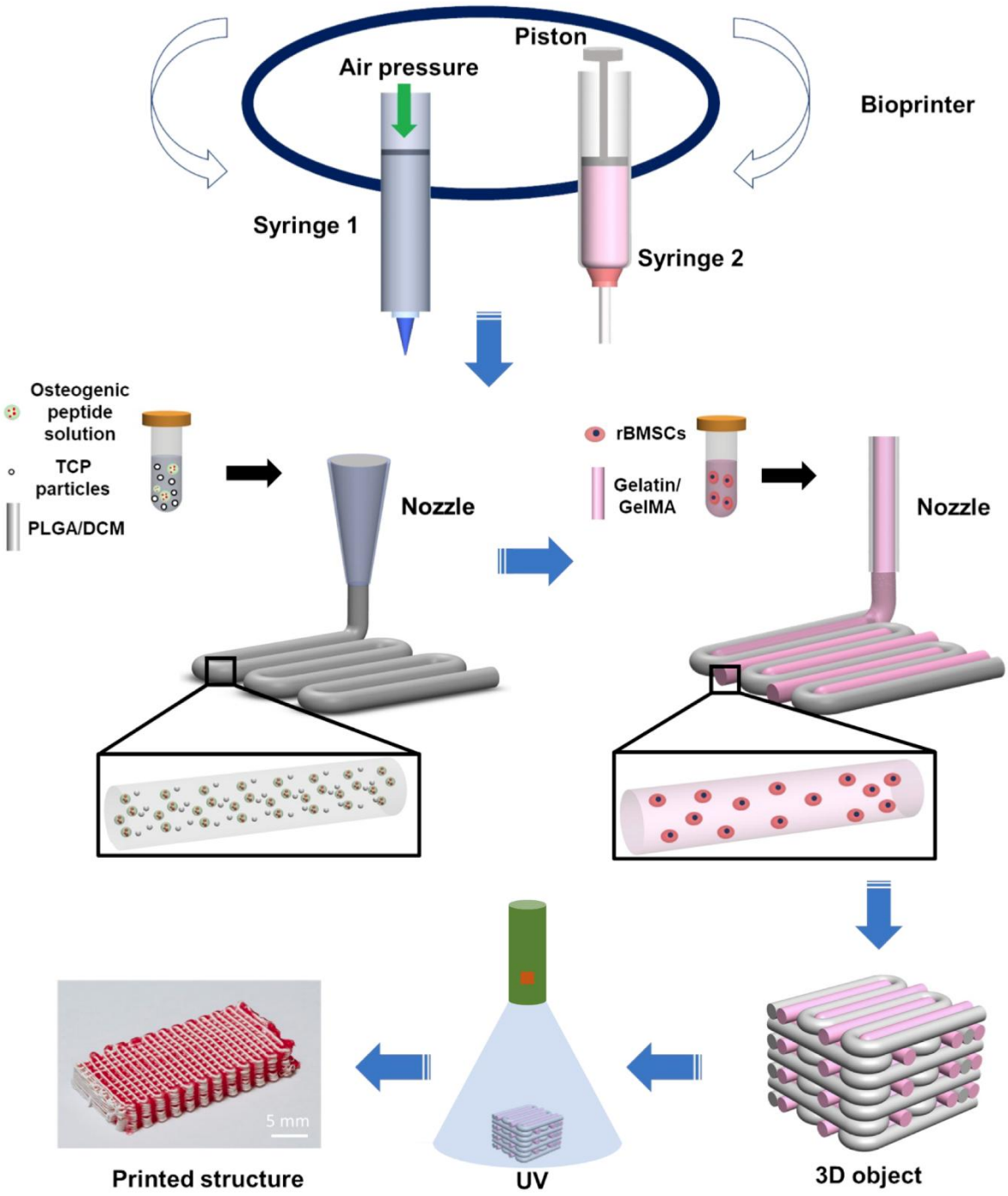

Fig. 1. Schematic illustration of the fabrication of GGOTP scaffolds with *in situ* delivery of OP and rBMSCs via low temperature hybrid 3D printing.

Characterizations of scaffolds

The macroscopic morphology of scaffolds was obtained using a digital single lens mirrorless (DSLM) camera (Z6, Nikon, Japan). The microstructure of scaffolds was observed using a confocal laser scanning microscope (CLSM, Leica TCS SPEII, Germany) by staining the OTP struts and the GG rods with Fluorescein isothiocyanate (FITC) and Rhodamine B, respectively. Besides, the microstructure of the scaffolds was also observed using a field emission scanning electron microscope (Hitachi S4800 FEG SEM, Japan). Briefly, the 3D printed scaffolds were frozen at -70 °C overnight and then freeze-dried for 2 days. Next, all the scaffold samples were coated with a thin layer of gold. The surface morphology and cross-sectional morphology were observed using SEM, in which the cross-sectioned samples were prepared by fracturing the scaffolds in liquid nitrogen. Compression tests were performed for the GG, OTP and GGOTP scaffolds using a mechanical testing machine (Instron 5848, UK) at room temperature (n = 5 for each type of scaffolds). Degradation kinetics of GG hydrogels, OTP and GGOTP scaffolds were investigated by immersing the pre-weight samples (n = 3 for each type of scaffolds) in PBS solution supplemented with 0.02% (w/v) sodium azide for up to 4 weeks. At pre-set time points (1, 2, 3, 4 weeks), the samples were taken out, rinsed and dried, and then their remaining weight was recorded. The degradation behavior was evaluated by calculating the ratio between the remaining weight and the initial weight of each sample.

In vitro release behaviors of OP

To study the *in vitro* release behavior of OP, OP-FITC (i.e., OP was grafted with FITC), was used to replace OP to fabricate the hybrid scaffolds. 50 mg of OP-FITC loaded scaffold sample was added into 15 mL centrifuge tubes which were further added with 3 mL of PBS solution (pH 7.4) supplemented with 0.02% (w/v) sodium azide. The tubes were then put in a shaking water bath and the temperature was maintained at 37 °C. During a 24-day test period, at pre-determined time intervals, the release test liquid was taken out and the concentration of OP-

FITC in the test liquid was measured using a fluorescence microplate reader. Afterwards, fresh PBS solution with the same volume was added in the tubes for continuous incubation. The release behavior of OP was obtained by plotting cumulative release curve of OP in 24 days.

Release of unmodified gelatin from Gelatin/GelMA (GG) hydrogel

The *in vitro* release behavior of unmodified gelatin from UV crosslinked GG hydrogel was investigated following an established protocol [38]. Briefly, 400 μL of GG hydrogel precursor containing 5% (w/v) unmodified gelatin, 5% (w/v) GelMA and 0.2% (v/v) (2-Hydroxy-2-methylpropiophenone) was casted into a disc, followed by UV crosslinking for 30 s. Meanwhile, a disc with 200 μL of water containing 5% (w/v) GelMA was prepared in the same way and set as a control. Both samples were transferred to separate plastic tubes containing 10 mL of sodium chloride (NaCl) solution (13.7 mM) with 0.02% (w/v) sodium azide. The plastic tubes were then put in a shaking water bath at 37 °C for up to 72 h for gelatin release. At pre-set time points, 1 mL of supernatant was collected and replaced with the same amount of fresh NaCl solution. The gelatin concentration of the collected solutions was determined in a 96-well plate using the Pierce^{TM} Bicinchoninic Acid (BCA) Protein Assay Kit (Thermo Fisher Scientific, USA). Gelatin solutions with different concentration were prepared for establishing the standard curve. Each well was incubated at 37 °C for color development, and the absorbance of each well was measured using a microplate reader at the wavelength of 562 nm. The gelatin concentration of each collected solution was calculated according to the standard curve and then was used to establish the cumulative release profile of gelatin from the GG hydrogels.

Cell viability

The cell viability of printed cell-laden scaffolds was examined using a Live/Dead assay at specific time points, including (1) right after fabrication of cell-laden scaffolds, (2) after culturing cell-laden scaffolds for 3 and 7 days. For cell staining, cell-scaffold constructs were washed with sterilized PBS and then stained with PBS containing 4 μM EthD-1 and 2 μM calcein AM. The cell-laden scaffolds were incubated at room temperature for 20 min, in which live cells and dead cells were stained with green color and red color, respectively. Fluorescence images of the cell-laden scaffold constructs were obtained using a fluorescence microscope (Leica DMi8, Germany). The release of rBMSCs from GG hydrogel and their migration to the OTP struts can be also observed by conducting the Live/Dead assay at pre-designed time intervals. Post cell seeding on the GGOTP scaffolds was also performed to compare the effect of post cell seeding and *in situ* cell printing on the distribution of rBMSCs onto the OTP struts of GGOTP scaffolds.

Analyses of cell density and cell distribution

The cell density was calculated by measuring the cell fraction (*U*) via the following equation:

$$U = \frac{A_c}{A_s} \qquad (1)$$

where *Ac* and *As* are the total cell area and total area of the selected location of the scaffold, respectively.

The cell distribution was quantitatively assessed using the following equation:

$$CDI(\%) = 100 \times \left[1 - \frac{\sum_{i=1}^{N} |U_i - \bar{U}|}{N\bar{U}}\right] \qquad (2)$$

where *CDI* is referred to cell distribution index, *U* is the cell area fraction which is shown in equation 1, $\bar{U}$ is the average value of *N* cell area fractions. Typically, cell-scaffold constructs were *in vitro* cultures for 3-day and 7-day. At each time point, three cell-scaffold constructs

were subjected to a Live/Dead staining. Afterwards, ten fluorescence images (10×) were captured at random locations for each cell-scaffold construct using the inverted fluorescence microscope and then were post-processed using ImageJ. Each image was converted into an 8-bit binary image to isolate the cells from the image. Finally, the cell distribution index was determined using equation 2 (N = 10 images for each cell-scaffold construct).

MTT assay

MTT assay was performed to observe the cell proliferation on the scaffold constructs with or without OP. Briefly, at specific time points (day 1, 3 and 7), the scaffolds were washed with sterilized PBS and then immersed in 330 μL mixture containing 300 μL culture medium and 30 μL MTT solution (5 mg/mL in PBS), followed by culture at 37 °C for 4 h. Subsequently, 200 μL MTT mixture was removed and replaced with 300 μL dimethyl sulfoxide (DMSO) for dissolving the formed formazan crystals, followed by culture at 37 °C for 10 mins. Finally, 100 μL solution was transferred to 96-well plates and the MTT absorbance was read using a microplate reader (UVM 340, Asys HiTech GmbH, Austria) at the wavelength of 570 nm.

ALP expression

ALP staining was performed to investigate the osteogenic differentiation of the cell-laden scaffold constructs after *in vitro* culture for up to 14 days. The cells seeded onto the scaffold constructs were fixed and stained using the ALP staining kit (Wuxi puhe Biomedical Technology Co., Ltd, China). The stained constructs were observed using a DSLM camera (Z6, Nikon, Japan) and a stereo light microscope (RuiHoge, Nanjing Nanpai Technology Co., Ltd., China). Also, the ALP expression was quantified by investigating the ALP activity of rBMSCs on the scaffolds following the manufacturer's protocol (Beyotime Biotechnology Ltd, China).

Cell mineralization

During *in vitro* culture, part of the cells released from GG rods migrated to the surface of OTP struts, while part of them directly precipitated to the bottom of the culture dish and were co-cultured with the GGOTP scaffolds for 21 days. Afterward, Alizarin Red S (ARS) staining assay was performed to investigate the mineralization of rBMSCs precipitated onto the bottom of the culture dish. The reason why not directly performing ARS staining for the rBMSCs migrated onto the OTP strut surface was that: it was highly difficult to distinguish whether the stained area was induced by the cell mineralization or the presence of TCP nanoparticles (containing large amount of calcium salts) on OTP strut surface. For the ARS staining, briefly, the GGOTP scaffolds were taken out and the culture dish was washed twice using PBS. Then, the precipitated cells onto the bottom of the culture dish were fixed using 4% (w/v) paraformaldehyde (PFA) for 30 min at room temperature. Subsequently, after washing twice with PBS, the fixed cells were stained with ARS solution [2% (w/v), pH = 4.2] for 30 min. With further washing with PBS, the stained cells were observed using a stereo light microscope (RuiHoge, Nanjing Nanpai Technology Co., Ltd., China). After taking micrographs, 10% cetylpyridinium chloride (a Sigma-Aldrich product) was used to dissolve the nodules and the ARS quantification was examined at 562 nm.

Statistical analysis

All statistical analyses were performed using the SPSS software (version18). Numerical data are presented as the mean value ± standard deviation (S.D.). For the statistical comparisons, one-way analysis of variance (ANOVA) with the Student's t test was applied. $p < 0.05$ (*) was considered to be statistically significant, in which (*) was used to indicate the significant differences in histological images.

RESULTS

Scaffold design

Through cryogenic 3D printing, hierarchically porous bioceramics/polyester composite scaffolds incorporated with functional peptide in situ have been successfully fabricated, showing excellent mechanical strength and bone forming ability [6, 34]. However, seeding cells in such scaffolds to achieve a uniform cell distribution and high cell density is still challenging. In order to improve the initial cell distribution in OTP scaffolds and hence accelerate the bone repairing/regeneration, biomimetic bone tissue engineering scaffolds with dual delivery of OP and MSCs *in situ* were designed and fabricated via a low temperature hybrid 3D printing strategy, in which cell-laden GG hydrogels were printed in the gaps among paralleled OTP struts in each layer. Crosslinked GG rods with excellent biocompatibility can provide cells with a comfortable environment for temporary cell storage and subsequent cell release along with the degradation of GG matrices during culture, while OTP struts with suitable mechanical properties and hierarchical porous structure can act as a mechanically stable biomimetic platform for cells to migrate to and attach to, and further release OP to improve cell proliferation and osteogenic differentiation, hence improving the new bone formation.

Rheological properties of printing inks

The rheological properties of the OTP emulsion ink and GG bioink were investigated in terms of their shear viscosity as well as loss and storage modulus. For shear viscosity testing (Fig. 2a), it was observed that both emulsion and bioink exhibited decreased viscosity with increased shear rate, that is, shear-thinning behavior. The shear-thinning feature enabled the inks or bioinks to pass through a nozzle smoothly when large shear stress was applied and to generate stable filaments when the shear stress was removed [39, 40]. Besides, the OTP emulsion exhibited a higher viscosity than the GG bioink across the entire shear rates. For angular frequency sweep (Fig. 2b), it could be seen that both emulsion ink and bioink showed higher

storage modulus (G') than loss modulus (G"), indicating their gel-like states, which were beneficial for micro extrusion-based 3D printing [41].

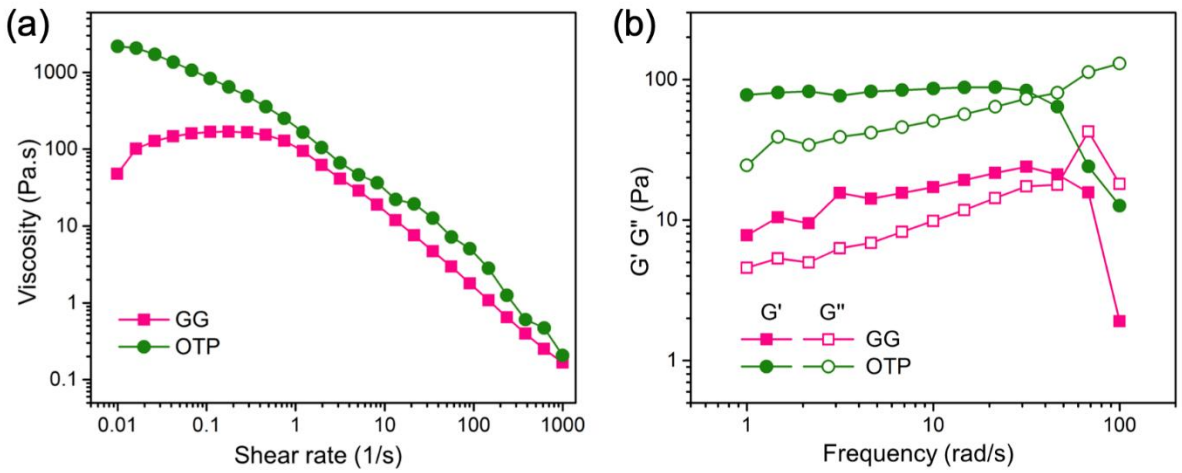

Fig. 2. Rheological properties of the OTP emulsion ink and GG bioink. (a) shear viscosity as a function of shear rate; and (b) storage and loss modulus as a function of frequency.

Morphology and structure of hybrid cell-laden scaffolds

The morphology and structure of the printed OTP and GGOTP scaffold constructs are shown in Fig. 3. As shown in Fig. 3a, OTP/DCM inks showed good printability, which allowed them to be printed into regular grid structures with 20 layers at 5 °C (thickness: 3.8 mm, pore size: 1.2 mm). In comparison, for the GGOTP scaffolds, GG hydrogel, stained with red food dye for better visualization, could be printed into the small gaps among paralleled OTP struts and almost fulfill the space of the gaps. Owing to the good printability of both OTP inks and GG bioinks, the GGOTP scaffolds could also be printed into 20-layered structures. Besides, CLSM was employed to observe the microstructure of the GGOTP scaffolds. It could be seen that the porous GG hydrogel (color in red) was accurately filled in the gaps among OTP struts (color in green) (Fig. 3b). Meanwhile, the top view and cross-sectional view of the GG hydrogel rods, OTP struts and GGOTP scaffolds were also observed using SEM to investigate the microstructures (Fig. 3c). It can be seen from the top and side views that GG hydrogel patterns

exhibited a typical hydrogel feature (i.e., showing a porous network structure after freeze drying treatment) while the OTP scaffolds exhibited a hierarchical porous structure consisting of both macroscopic grid pores and micropores on the rod/strut surface, which were consistent with that in a previous study [33]. It should be noted that the OTP struts of the GGOTP scaffolds also exhibited a hierarchical porous structure which was similar to that of the OTP scaffolds, indicating that simultaneously printing of GG bioink and OTP ink had little side-effect on the formation of micropores on OTP strut surface during the low temperature hybrid 3D printing. The cross-sections of both types of OTP and GGOTP scaffolds also showed little difference on the region of the OTP struts, indicating that the inner structure of OTP struts was not affected even after the deposition of GG hydrogel rods. Besides, SEM micrographs of cross-sectioned GGOTP scaffolds showed that GG hydrogel rods with a typical porous network structure was accurately deposited into the spaces/gaps of the parallel OTP struts according to the CAD design, indicating an excellent fabrication accuracy of our low temperature hybrid 3D printing technology.

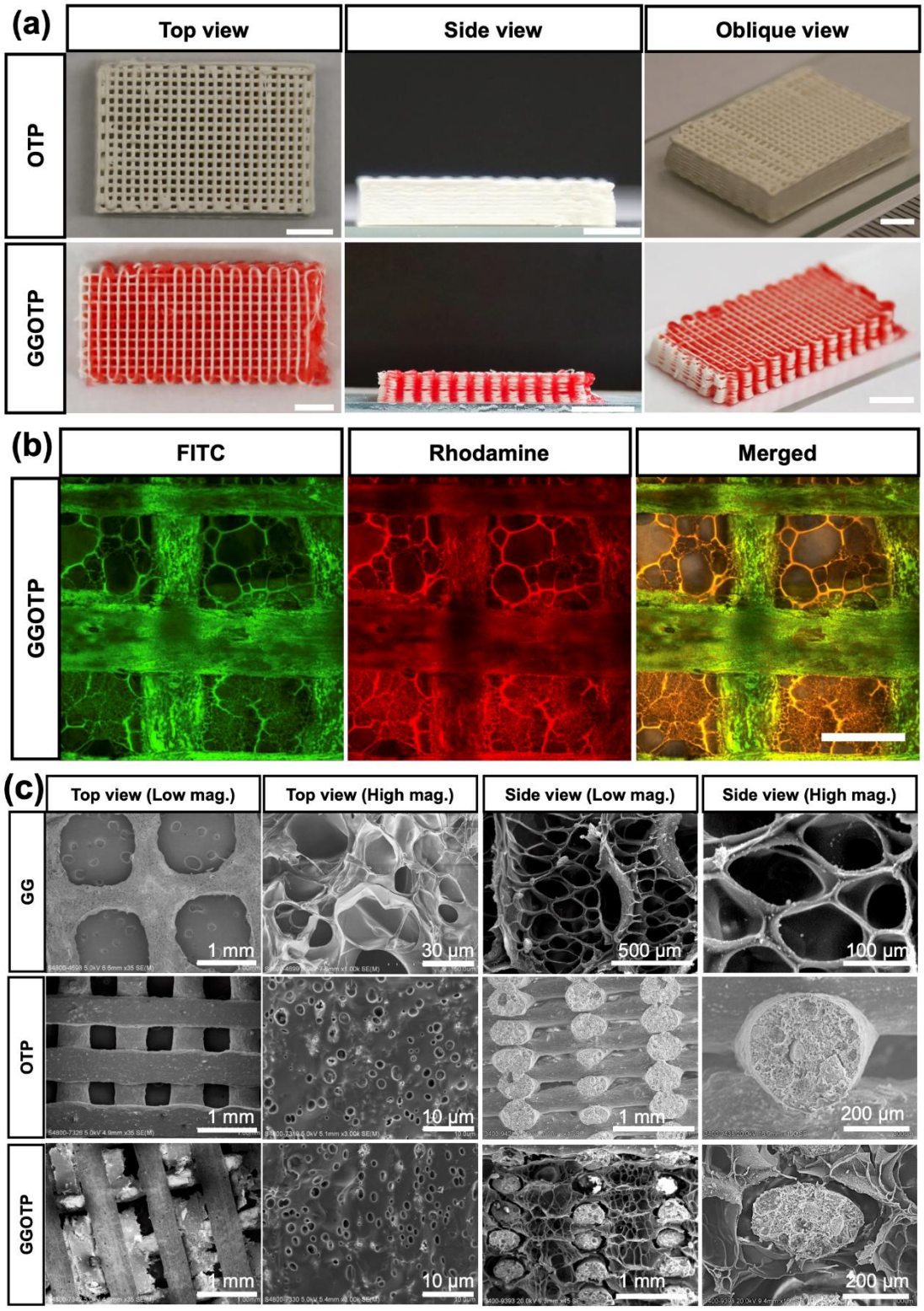

Fig. 3. Morphology and structure of the printed scaffolds: (a) photographs of the single printed OTP constructs and hybrid printed GGOTP constructs (scale bar: 5 mm); (b) fluorescence

images of the hybrid printed GGOTP constructs (scale bar: 1 mm); (c) SEM images of the GG hydrogels, single OTP constructs and hybrid GGOTP constructs with top view and side view.

Mechanical properties of scaffolds

The mechanical properties of different scaffolds (i.e., GG, OTP and GGOTP) were evaluated using compression testing. The typical stress-strain curves are shown in Fig. 4a. As shown in Fig. 4b and c, the GG scaffolds exhibited relatively low compressive strength (0.39 MPa) and elastic modulus (0.23 MPa). Such weak mechanical properties are a common problem in most scaffolds made of natural polymers such as alginate, hyaluronic acid, and fibrin [42-44]. Thus, single natural polymers normally are not suitable for the repairing of bone defects where load bearing is required. In comparison, OTP and GGOTP scaffolds had much higher elastic moduli (23.7 MPa and 19.6 MPa) and compressive strengths (16.7 MPa and 11.2 MPa), which are comparable to the human cancellous bone [45], suggesting that the cell-laden OTP scaffolds fabricated via low temperature hybrid 3D printing still had appropriate mechanical properties as an excellent platform for bone repairing/regeneration.

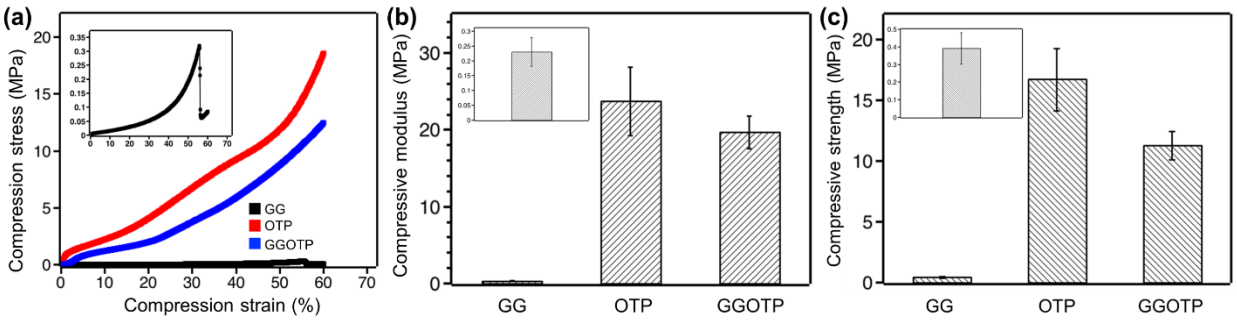

Fig. 4. Mechanical properties of the GG, OTP and GGOTP scaffolds: (a) compressive strain-stress curves, (b) compressive modulus, and (c) compressive strength. Inset is the zoom of GG's compression testing results.

Degradation and *in vitro* release behavior of OP from scaffolds

The *in vitro* degradation behavior of GG hydrogels, OTP scaffolds and GGOTP scaffolds was characterized by monitoring their weight remaining in a 4-week test period (Fig. 5a). GG hydrogels were completely degraded within 1 week and thus the data were not shown in Fig. 5a. For the OTP scaffolds and GGOTP scaffolds, they exhibited much slower degradation than GG hydrogels. Compared to the OTP scaffolds, the GGOTP scaffolds showed a higher weight loss, which can be attributed to the quick degradation of GG hydrogel rods within the GGOTP scaffolds. Nevertheless, GGOTP scaffolds remained about 81.6% of the initial weight after 4-week incubation, indicating the GGOTP scaffolds could keep their integrity to support the long-term bone regeneration.

Fig. S2 showed the *in vitro* release behavior of gelatin from the GG hydrogels for up to 72 h. Unmodified gelatin showed a quick release from the GG hydrogels and achieved a release level of 56% in 24 h. After 48 h of incubation, as high as 94% of gelatin was released. After 72 h of incubation, the entire unmodified gelatin was released from the GG hydrogels. The release of gelatin from GG hydrogel could be attributed to that the diffusion of gelatin (in the liquid state at 37 ^{o}C) from the GG hydrogels.

The *in vitro* release behavior of OP is shown in Fig. 5b. OP released from OTP scaffolds showed a bi-phasic release profile, consisting of an initial fast release up to 56% level in 3 days, followed by a slower but more steady release which reached 88% level at day 24. The initial OP release from OTP scaffolds could be attributed to the dissolution of OP located in the micropores on or near the strut surface. In comparison, the initial fast release of OP from GGOTP scaffolds was reduced to 32% in 3 days, and a more sustained OP release was obtained in 24 days, achieving a total release level of 78%. The reduced initial OP release level from GGOTP scaffolds could be attributed to following reasons: (1) the adjacent GG hydrogel rods hindered the direct release of OP into the test liquid; (2) some of the OP released from the OTP

struts diffused into the adjacent GG hydrogel rods. Along with the dissolution of GG hydrogel, OP release from GGOTP scaffolds was accelerated.

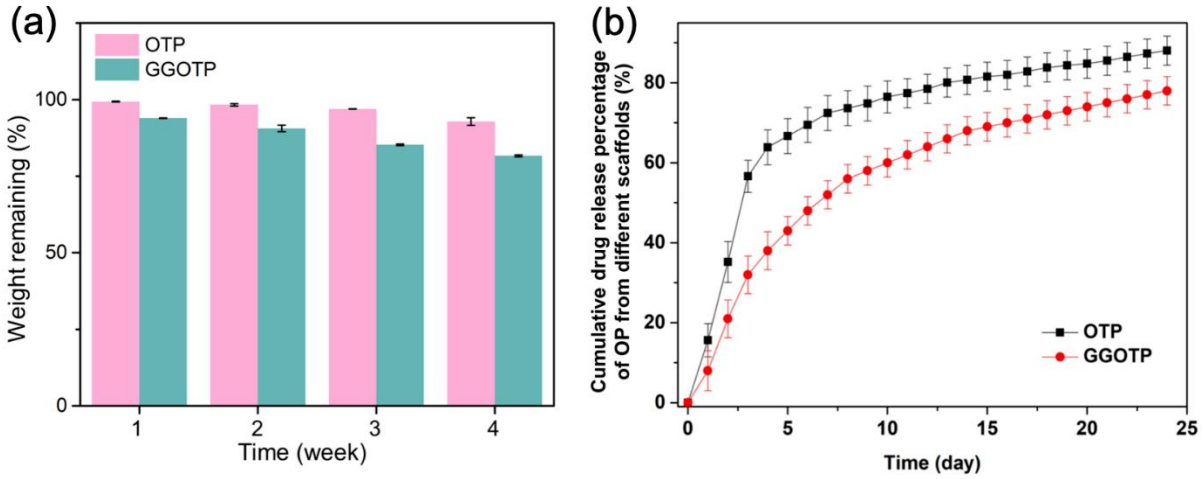

Fig. 5. (a) Degradation properties of OTP and GGOTP scaffolds. (b) *In vitro* release behavior of OP from different scaffolds.

Viability and proliferation of rBMSCs in two types of cell-laden scaffolds

Before the printing of GGTP and GGOTP scaffolds, the states of rBMSCs within the GG hydrogels with different cross-linking degrees were investigated, as shown in Fig. S3. On day 0, the cells in all GG hydrogels kept round in shape. GG hydrogels which were crosslinked for 0 s or 30 s degraded quickly after 1- and 3-day incubation, and the loaded cells were released concurrently and attached onto the substrate of the culture dish. It should be noted that GG hydrogels without crosslinking can release the cells in a much quicker pace than that crosslinked for 30 s. When GG hydrogels were crosslinked for more than 90 s, they could hold their structural integrity and nearly no cell release was observed within 3 days. Meanwhile, the cells within the hydrogels were still spherical in shape. Moreover, even after 7 days of *in vitro* culture, rBMSCs encapsulated in the GG hydrogels just exhibited little expansion (Fig. S4). Therefore, if the cells were encapsulated in the GG hydrogels with no release capability, they remained round in shape for a long time, which was not favorable for cell morphogenesis and

osteogenic differentiation for bone regeneration. In such cases, it would be more beneficial that the cells could be quickly released from the GG hydrogel rods and then migrated to the OTP struts, followed by cell spreading on the strut surface and differentiation along with the osteogenic linage. Considering the cell release and following migration to OTP struts, GG rods were UV crosslinked for 30 s when fabricating the GGTP and GGOTP scaffolds.

The cell viability and cell proliferation were investigated using one-layered GGTP and GGOTP scaffolds, as illustrated in Fig. 6a. The viability of rBMSCs in the cell-laden GGTP and GGOTP scaffolds was investigated using Live/Dead staining assay (live for green and red for dead), as shown in Fig. 6b and 6c. On day 0 (i.e., right after fabrication), few dead cells were observed in both types of cell-laden scaffolds, and GGTP and GGOTP exhibited a cell viability of 86.7% and 87.4%, respectively. These results suggested that rBMSCs in GG rods successfully withstood the low temperature hybrid 3D printing process in which DCM and cryogenic environment are usually considered as negative factors for cell survival[46]. In addition, rBMSCs laden in the GG hydrogels were still round in shape and homogeneously distributed in the gap of TP struts or OTP struts. After 3 days of culture, most of the living cells were released from GG hydrogel rods and migrated to the surface of TP or OTP scaffold struts, along with the almost completed dissolution of GG hydrogels. Also, it could be seen that the rBMSCs migrated to the struts exhibited obvious cell attachment, and were homogeneously distributed on strut surface, showing discernible cell spreading. These results indicated that the DCM in the TP or OTP struts were almost removed with the assistance of airflow in the 3D printing fume hood during the suspension of the printer. If the printed was not suspended after depositing the OTP struts and the cell-laden GG bioink was allowed to be directly filled into the gaps of “wet” OTP struts without delay, a slower DCM evaporation would occur, thereby leaving more residual DCM in the OTP struts. In such a case, the rBMSCs released from the GG rods would not attach to the surface of OTP struts due to the presence of more residual

DCM (Fig. S5). Furthermore, compared to the GGTP scaffolds, GGOTP scaffolds induced a slightly higher cell density on the OTP struts after 3-day culture, suggesting that the released OP from the OTP struts was beneficial for cell migration/cell anchorage to/on OTP struts. To verify this, MTT assay was performed to study the cellular metabolic activity as an indicator for cell proliferation (Fig. 6d). It was found that MTT absorbance was increased with the culture time for both scaffolds, while that for the cell-laden GGOTP scaffolds was significantly higher at day 3 than that for GGTP scaffolds, confirming live/dead observations.

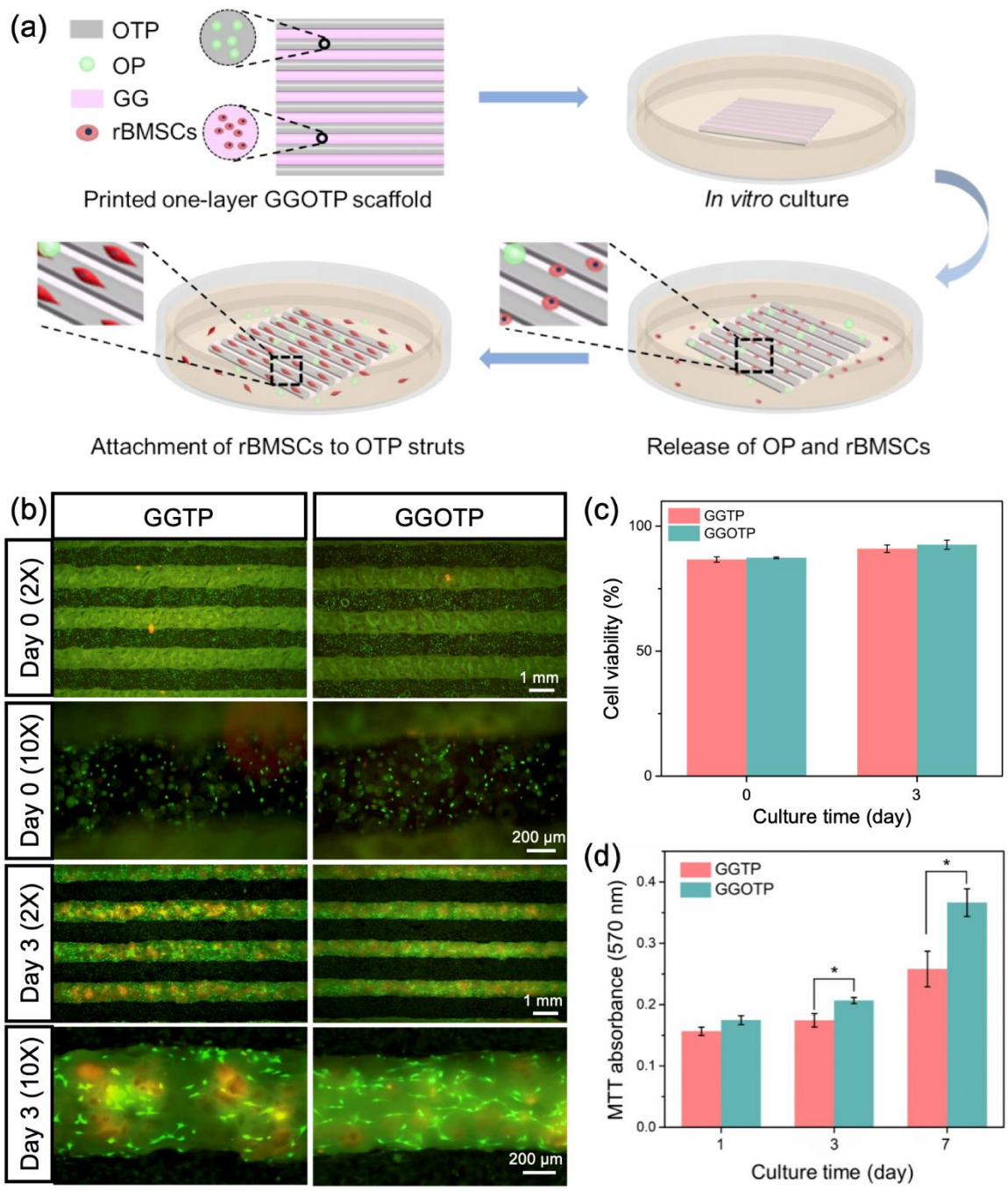

Fig. 6. Viability of rBMSCs in cell-laden scaffolds made through low temperature hybrid 3D printing: (a) schematic illustration of the cell behavior during *in vitro* culture; (b) live/dead images (at 2× and 10× magnifications) of rBMSCs in GGTP and GGOTP scaffolds at day 0 and day 3; and (c) their corresponding cell viability; (d) MTT absorbance of rBMSCs in GGTP and GGOTP scaffolds after 1-, 3- and 7-day culture.

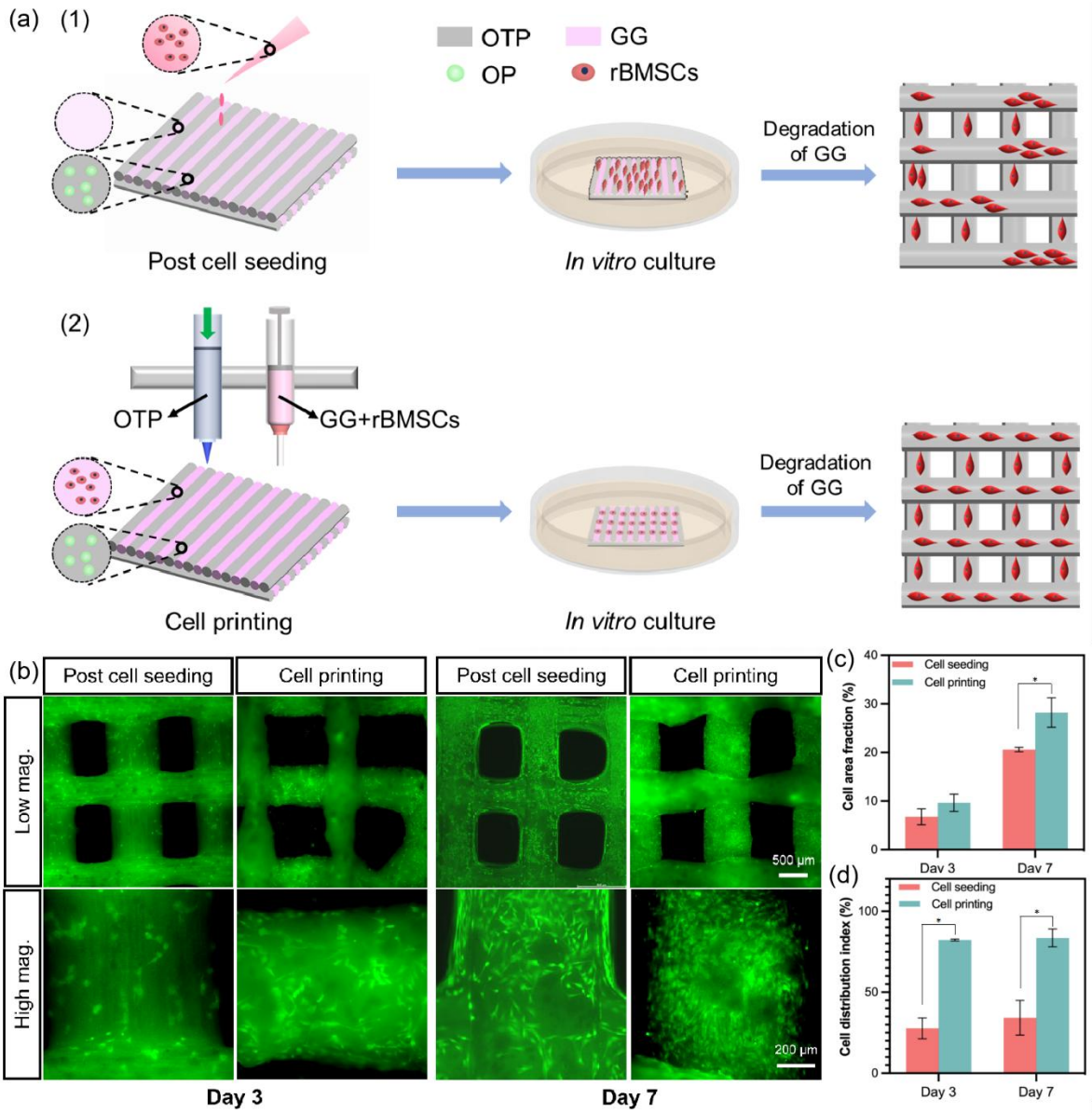

Fig. 7. Comparison of cell distribution onto the two-layer GGOTP scaffolds prepared via (1) post cell seeding and (2) *in situ* cell loading (i.e., cell printing). (a) Schematic illustration of these two strategies; (b) fluorescence images representing the cell viability, cell density and cell distribution onto the scaffolds after *in vitro* culture at day 3 and day 7; (c) histogram of cell area fraction; (d) histogram of cell distribution index.

Two-layered cell-laden GGOTP scaffolds were also successfully printed using the "dual-nozzle" low temperature hybrid 3D printing strategy. The GGOTP scaffolds treated with post-fabrication cell seeding strategy were prepared as well to compare the effects of post-

fabrication cell seeding and *in situ* cell delivery (i.e., cell printing) on the cell attachment and cell distribution on OTP struts (Fig. 7a). As can be seen from Fig. 7b, after 3- and 7-day culture, the density of rBMSCs on the struts made through the cell printing strategy was higher than that on the struts treated with post-fabrication cell seeding. In addition, the scaffolds treated with post-fabrication cell seeding showed varying cell densities in different regions of the struts after 3- and 7-day culture, while homogeneous cell distribution was observed on struts made through the cell printing strategy. The quantitative analysis results of cell density in terms of cell area fraction in different groups are presented in Fig.7c. Both types of scaffolds exhibited increased cell area fractions during *in vitro* incubation from day 3 to day 7, indicating a cell growth trend along with increased culturing time. Also, the cell-scaffold constructs made via the cell printing strategy exhibited higher cell area fractions, suggesting a higher cell density and better cell proliferation than those treated with the cell seeding strategy. To quantitatively measure cell distribution, the cell distribution index (*CDI*) of cell-scaffold constructs made through the two different strategies was calculated and presented in Fig.7d. It can be seen from Fig.7d that cells on the cell-scaffold constructs prepared via the cell printing strategy showed a much higher *CDI* value (82.3% and 83.53% for day 3 and 7, respectively) than those on the cell-scaffold constructs prepared via the cell seeding strategy (27.7% and 34.25% for day 3 and 7, respectively), suggesting a much more homogeneous cell distribution on the cell-scaffold constructs made through the cell printing strategy. The above results have demonstrated that simultaneously loading live cells in structures for tissue engineering during the 3D printing process is a feasible (and also better) approach to solve the problem of inhomogeneous cell distribution brought up by the post-fabrication cell seeding strategy.

Effect of sustained release of OP on the osteogenic differentiation of rBMSCs

Biomolecules such as BMP-2 and OP are important to promote bone repairing/regeneration and have a great influence in regulating the cells behavior (i.e., attachment, proliferation and osteogenic differentiation). To investigate the influence of OP release on the osteogenic differentiation of rBMSCs in scaffolds, ALP and ARS assays were performed for two types of cell-laden scaffolds with/without OP (GGOTP vs. GGTP), as shown in Fig. 8. The macroscopic images of ALP stained cell-scaffold constructs after 7-day culture are shown in Fig. S7. From the microscopic images (Fig. 8a and 8b), it was observed that GGOTP scaffolds exhibited improved ALP expression compared to GGTP scaffolds by showing more intensive blue area. The ALP activity assay results (Fig. 8e) also showed the same trend, demonstrating that sustained release of OP from the OTP struts could significantly improve the osteogenic differentiation of rBMSCs. Besides, the results of ARS staining showed that the rBMSCs (released from GG rods and then attached to the bottom of the culture dish via sedimentation) co-cultured with GGOTP scaffolds exhibited a larger calcium deposition area (color in dark red) than that cultured with GGTP scaffolds (Fig. 8c and 8d). The quantitative analysis of ARS stained calcium nodes also verified the same trend (Fig. 8f), indicating that the sustained release of OP could stimulate significantly increased cell mineralization. These results demonstrated that compared to the scaffolds without OP, *in situ* delivery of OP could greatly improve the bone forming activity of cell-laden TCP/PLGA scaffolds and contribute to the osteogenic differentiation of rBMSCs.

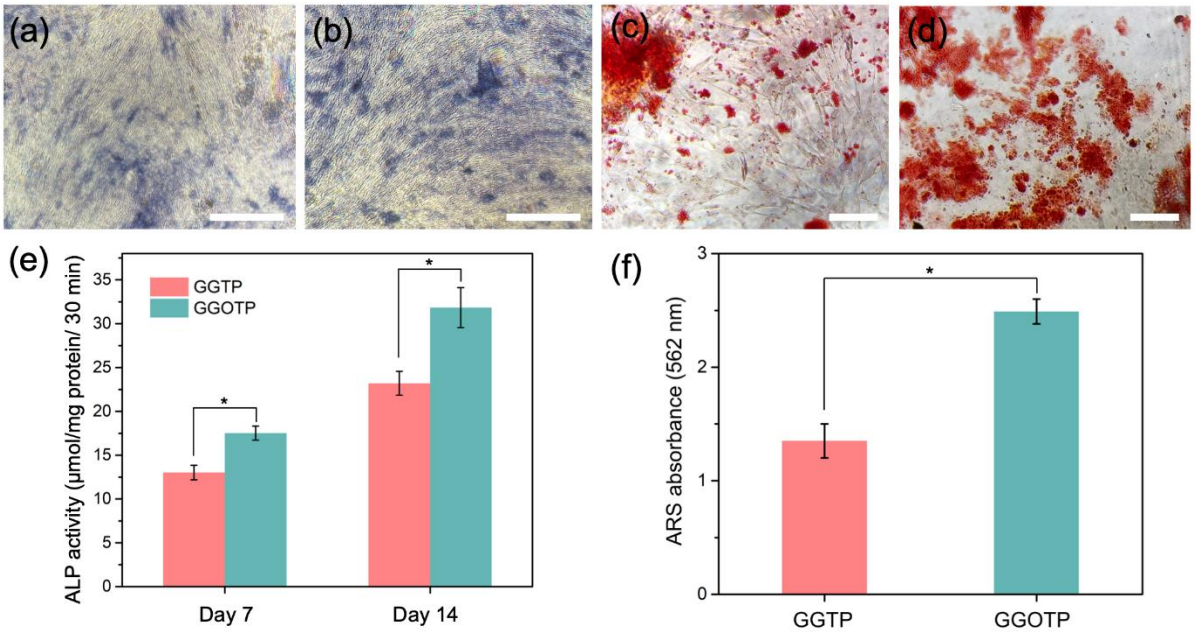

Fig. 8. Osteogenic differentiation of rBMSCs in GGTP and GGOTP scaffolds. (a, b) ALP staining (blue area) of rBMSCs for the (a) GGTP scaffolds and (b) GGOTP scaffolds after 14-day *in vitro* culture; (c, d) ARS staining of rBMSCs (released from the GG rods and then precipitated onto the substrate of the culture dish) for the (c) GGTP scaffolds and (d) GGOTP scaffolds after 21-day *in vitro* culture; (e) ALP activity of rBMSCs for GGTP and GGOTP scaffolds for up to 14 days; (f) quantitative analysis of the dissolved calcium nodules after 21-day *in vitro* culture (Scale bar: 100 μm).

DISCUSSION

Successful bone tissue engineering requires a number of key factors, including biodegradable and biocompatible 3D scaffold with a pre-designed structure which is structurally and mechanically similar to the ECM of human bone tissue, the appropriately loaded seed cells which have capabilities of proliferation and osteogenic differentiation, and suitably incorporated bioactive agents, especially growth factors and equivalent peptides which can elicit desirable cell responses and direct cell differentiation. Compared to conventional fabrication techniques, 3D printing is advantageous in producing bone tissue engineering

scaffolds with personalized shape, tailored pore size/porosity, required mechanical properties, etc. Scaffolds made of bioceramics (e.g., TCP, hydroxyapatite or bioactive glass) [20, 47], polymers (either synthetic polymers such as PLA and polycaprolactone or natural polymers such as gelatin, alginate and hyaluronic acid) [3, 18, 23]and their composites [5, 15, 24] have been successfully produced via 3D printing such as SLS, FDM and micro extrusion-based 3D printing. However, it is relatively difficult to give consideration to the successful 3D printing of scaffolds with desirable features and efficient cell loading at the same time, since uniform distribution of cells in scaffolds with a complex shape and structure is relatively difficult via post-fabrication cell seeding strategy. Usually, 3D printed synthetic polymeric scaffolds could only be seeded with cells after the scaffold fabrication process, as the direct loading of cells and/growth factors during the fabrication process would result in significantly lowered cell viability/growth factor biological activity owing to harsh processing conditions (e.g., heat in FDM, laser in SLS, and organic solvent used in micro extrusion-based printing) during the fabrication process. To overcome these limitations, bioprinting which could print cell-laden and growth factor-loaded hydrogel trajectory/scaffolds has been developed [48, 49]. However, drawbacks such as limited mechanical strength, insufficient microporous features on strut surfaces still exist, lowering its effectiveness in inducing bone tissue regeneration. To this end, a novel 3D printing strategy which could enable the production of scaffolds with sufficient mechanical strength, hierarchical porous structure and capability of *in situ* delivery of growth factor and seed cells should be developed.

Researchers have employed a “dual-nozzle” hybrid 3D printing technology to produce cell-laden synthetic polymer/hydrogel scaffolds, in which synthetic polymer with a low melting point was thermally extruded to form scaffold supports, while cell-laden hydrogel was extruded and filled between paralleled synthetic polymer struts [3, 31]. However, the extruded synthetic polymeric struts lacked surface roughness and micropores for easy cell attachment and growth

factors could only be loaded in the hydrogel which was relatively difficult to achieve a long-term sustained release. To address these limitations once for all, in the current study, low temperature hybrid 3D printing was developed. The advantages of low temperature hybrid 3D printing include: (1) ability to simultaneously process emulsion ink and bioink into cell-laden scaffolds; (2) stabilization of the GG and OTP struts during printing at the low temperature environment; (3) formation of mechanically strong and hierarchically porous scaffolds with interconnected macropores and micropores on the OTP struts; (4) incorporation of biomolecules such as OP and living cells into the scaffolds during the printing process, which cannot be achieved by other 3D printing technologies such as SLS and FDM solely since they involve high temperatures during the fabrication process; (5) formation of cell-laden scaffold constructs with a uniform cell distribution. During the low temperature printing process, the as-printed GG hydrogel rods had a double-network structure, with a helical gelatin network induced by the low temperature environment and a free radical polymerized network induced by the UV irradiation. When culturing the GGOTP scaffolds at 37 °C, the physically gelated gelatin in the GG hydrogel rods became soluble and hence GG hydrogels became single-network hydrogels. Compared to other cell-laden hydrogel scaffolds in which cells are permanently located at fixed positions, when employing GG hydrogel instead of GelMA solely as the hydrogel matrix, rBMSCs can be released quickly from the closed hydrogel environment along with the dissolution of gelatin, and further freely migrate to the surface of OTP struts nearby. Meanwhile, the hierarchically porous OTP struts in which OP was gradually released can act as excellent destination for cell migration, cell anchorage and cell spreading, and further elicit osteogenic differentiation.

People may also concern about the necessity of developing such an advanced low temperature hybrid 3D printing strategy, as infusing cell-laden hydrogel precursors into 3D printed OTP scaffolds with an open porosity, followed by UV crosslinking, seems to have the same effect

on obtaining cell-laden GGOTP scaffolds. However, if porous OTP scaffolds were 3D printed first and then infused with cell-laden hydrogels, several problems would be encountered:

(1) In such an operation, some (maybe a lot, depending on particular situations) cell-laden hydrogel precursors would be leaked out from OTP scaffolds through open pores during the infusion of cell-laden hydrogel precursors, resulting in wastage of precious cells, particularly stem cells.

(2) The cell-laden hydrogel precursors may not totally infuse the 3D printed OTP scaffolds. This is a complicated situation which is influenced by several factors. Exerting high pressure for total infusion may cause cell death. Extending the infusion time for achieving an even and total infusion may also cause cell death.

(3) The hydrogel precursors filling the gaps among paralleled OTP struts with an X-direction in the X-Y plane cannot be fully cured by UV irradiation due to the sheltering effect of the OTP struts with a Y-direction in the X-Y plane located at the upper layer if the UV irradiation is applied from the top of the scaffold, thus forming cell-laden hydrogel struts with alternately distributed fully crosslinked segments and not fully crosslinked segments. This will cause cell release problems.

(4) Cell segmentation may occur during infusion and also during the UV irradiation process as the cell-laden hydrogel precursors could easily flow, thus causing inhomogeneous cell distribution in the vertical direction if the precursors are fed from the top for infusion.

In the current investigation, by employing the low temperature hybrid 3D printing strategy, the cell-laden hydrogel precursors can be precisely placed in pre-determined positions, which will improve the utilization efficiency of the cell-laden hydrogels and reduce the waste of seed cells. Since cell-laden hydrogel precursor rods printed at each layer had a fixed layer thickness (hundreds of microns), fast and uniform crosslinking of cell-laden hydrogel precursor rods can

be achieved via UV irradiation of a short duration, and no discernible cell segmentation will occur. This strategy is favorable for maintaining cell viability and achieving homogeneous cell distribution. In summary, the strategy developed in the current study has enabled us to produce a cell-containing hybrid scaffold with a uniform cell distribution, a homogeneous hydrogel crosslinking density in a more cost-effective way.

It is worth noting that the viability of rBMSCs was well maintained during the low temperature hybrid 3D printing process and the subsequent cell culture process. Given that DCM which was used to formulate printing inks for producing OTP scaffolds is cytotoxic and the low temperature environment may lead to cell death due to the formation of ice crystal in cells, whether rBMSCs loaded in GG hydrogel patterns were alive or not is highly concerned. The key issues to maintain the high cell viability during low temperature hybrid 3D printing are to reduce the DCM content in the as-printed OTP patterns before the deposition of rBMSC-laden GG hydrogel pattern and prevent the ice formation in cells. Towards the risk brought by DCM, in the current investigation, the printing program was carefully controlled to provide a sufficient long time interval between the 3D printing of OTP struts and cell-laden GG hydrogel rods, to ensure that the DCM can be mostly evaporated. Besides, as concentrated composite emulsion inks (i.e., 3 g of TCP and 3 g of PLGA were blended with 10 mL of DCM and 1-2 mL of DI water to form viscous slurry) were used to draw the OTP struts and the as-extruded OTP struts only had a diameter of 0.4 mm, nearly all DCM had been removed from the OTP struts already with the assistance of an airflow in the 3D printing fume hood due to its very high volatility, when the GG rods were filled in the gaps of paralleled OTP struts. Towards the risk brought by cryogenic environment, the GGOTP scaffolds printed under -20 °C showed no cell survived after *in vitro* culture for 3 days (Fig. S6), suggesting that a too low temperature would definitely kill cells. Therefore, in the current study, the temperature of the cryogenic stage was set as 5 °C instead of -30 °C which was employed in our previous studies to avoid

ice formation in cells. Since the OTP/DCM emulsion inks had a very high viscosity, the low temperature environment of 5 °C was sufficient to stabilize the as-extruded OTP struts. With the assistance of airflow during the low temperature hybrid 3D printing process, DCM can be quickly evaporated and hence the OTP struts can be fully solidified to show suitable mechanical strength at 37 °C.

The incorporation of biomolecules such as growth factors and equivalent peptides into the 3D printed cell-laden scaffolds endows them capabilities of stimulating cell growth and differentiation and thus improve the bone regeneration. There may exist some non-specific physical interactions between the OP and TCP/PLGA composite matrices. It should be also noted that there was nearly no loss and inactivation of OP during the low temperature printing process since the printing environment was mild. With above considerations, the loading efficiency of OP into the OTP struts was assumed to be nearly 100%. The fast initial OP release from OTP and GGOTP scaffolds could contribute to obtaining therapeutical concentration quickly, while the sustained release could contribute to the long-term stimulation on bone regeneration. Moreover, the released OP promoted the migration and anchorage of cells (released from GG hydrogel rods) towards the OTP struts. Thirdly, GGOTP scaffolds exhibited significantly better cellular metabolic activity than GGTP scaffolds, suggesting that the released OP contributed to cell proliferation. Fourthly, the released OP facilitated the osteogenic differentiation of rBMSCs by showing enhanced ALP expression and improved cell mineralization. Finally, in the current study, OP was physically immobilized into the polymeric structures via weak physical interaction (e.g., hydrogen bonding). Such physical immobilization had nearly no effect on the performance of OTP scaffolds in terms of hierarchically porous structure, degradation kinetics, and mechanical properties [6, 50]. If OP was functionalized in the polymeric structure, the release profile should be different. In that situation, OP release may be much slower than that of the method we used in this study [51,

52]. This is because OP needs to break the linkage with the polymeric matrix before releasing from the polymeric structure, which slows down OP release. Compared to the possible surface functionalization strategy, direct incorporation of OP into the OTP scaffolds has following advantages: (1) easy operation without taking any chemical reaction to link the OP to the polymeric matrix; (2) high loading efficiency and loading amount which are hardly to be achieved via the surface functionalization strategy; (3) little side effect on the biological activity of OP, whereas in the functionalization strategy, possible hazards substances may be used during functionalization reaction between OP and the polymer matrix, leading to decreased activity of OP. The developed cell-laden GGOTP scaffolds with *in situ* delivery of OP and rBMSCs exhibited excellent performance: hierarchically porous structures with interconnected macropores and micropores, mechanical modulus of about 19.6 MPa, sustained release of OP, and homogeneous distribution of cells onto each OTP struts. The performance of GGOTP scaffolds is comparable to that of human cancellous bone, which has a spongy-like structure with a porosity of 50-90% and mechanical modulus of 0.02-2 GPa [13, 53, 54]. Therefore, these results suggest that the low temperature hybrid 3D printed GGOTP scaffolds can be used to fill the bone defects at non-weight-bearing regions (e.g., cranial defect of rats, non-load bearing part of distal rabbit femur). It has been demonstrated that cryogenic 3D printed OTP scaffolds greatly improved bone regeneration in rat cranial defects compared to TP scaffolds [6, 34]. Therefore, in our future work, it can be expected that implanting GGOTP scaffolds with *in situ* cell delivery into the rat cranial defects can better facilitate bone regeneration compared to OTP scaffolds solely. Besides, the *in vivo* performance of GGOTP scaffolds prepared via post-cell seeding and *in situ* cell delivery should also be carefully compared.

CONCLUSIONS

In this study, cell-laden gelatin/GelMA (GG)-OP/TCP/PLGA (GGOTP) nanocomposite scaffolds with a homogeneous hydrogel crosslinking density and a uniform cell distribution were cost-effectively produced through low temperature hybrid 3D printing. The scaffolds were hierarchically porous and mechanically similar to human cancellous bone. rBMSCs incorporated in GGOTP scaffolds showed high viability after 3 days of culture and these scaffolds supported cell proliferation, with better metabolic activity being observed in GGOTP scaffolds as compared to the control groups. These scaffolds were also found to improve the osteogenic differentiation of rBMSCs by showing enhanced ALP expression during a 14-day period and enhanced calcium deposition during a 21-day period. This study provided a facile "one-step" strategy in 3D printing to construct cell-laden composite scaffolds with biomimetic structure, superior mechanical properties, enhanced bone forming ability, *in situ* biomolecule and cell delivery capability for improved bone tissue regeneration.

ACKNOWLEDGEMENTS

This work was financially supported by Guangdong Basic and Applied Basic Research Foundation (2019B1515130005), KEY Laboratory of Robotics and Intelligent Equipment of Guangdong Regular Institutions of Higher Education (2017KSYS009), Guangxi Science and Technology Program (Guike Jizi [2020] No. 198), Department of Education of Guangdong Province, China (2021ZDZX2014), Key Science and Technology Project of Social Development Foundation of Dongguan, China (20211800904542, 20211800904612), National Science Foundation of China (52173148, 82171997), Natural Science Foundation of Guangdong Province, China (2018A030313923). J. Lai and S. Chen thank The University of Hong Kong (HKU) for awarding them with a PhD scholarship which enables them to conduct research at HKU. M. Wang acknowledges the grant support (GRF17201017, 17200519 and 17202921) from the Research Grants Council of Hong Kong and HKU's support through grants in the Seed Fund for Basic Research Programme. M. Wang's research in biomaterials and tissue

engineering is also supported by a donor in Hong Kong through her generous donation. Assistance provided by Xiaodie Chen in M. Wang's group at HKU and by technical staff in HKU's Department of Mechanical Engineering and Electron Microscopy Unit is acknowledged.

REFERENCES

[1] Chua C K and Yeong W Y 2014 *Bioprinting: principles and applications* vol 1: World Scientific Publishing Co Inc)

[2] Lanza R, Langer R, Vacanti J P and Atala A 2020 *Principles of tissue engineering*: Academic press)

[3] Park J Y, Shim J-H, Choi S-A, Jang J, Kim M, Lee S H and Cho D-W 2015 3D printing technology to control BMP-2 and VEGF delivery spatially and temporally to promote large-volume bone regeneration *Journal of Materials Chemistry B* **3** 5415-25

[4] Wang C, Zhou Y and Wang M 2017 In situ delivery of rhBMP-2 in surface porous shape memory scaffolds developed through cryogenic 3D plotting *Mater. Lett.* **189** 140-3

[5] Yang Y, Zhang Q, Xu T, Zhang H, Zhang M, Lu L, Hao Y, Fuh J H and Zhao X 2020 Photocrosslinkable nanocomposite ink for printing strong, biodegradable and bioactive bone graft *Biomaterials* **263** 120378

[6] Wang C, Lai J, Li K, Zhu S, Lu B, Liu J, Tang Y and Wei Y 2021 Cryogenic 3D printing of dual-delivery scaffolds for improved bone regeneration with enhanced vascularization *Bioactive Materials* **6** 137-45

[7] Hua M, Wu S, Ma Y, Zhao Y, Chen Z, Frenkel I, Strzalka J, Zhou H, Zhu X and He X 2021 Strong tough hydrogels via the synergy of freeze-casting and salting out *Nature* **590** 594-9

[8] Moon J Y, Lee J, Hwang T I, Park C H and Kim C S 2021 A multifunctional, one-step gas foaming strategy for antimicrobial silver nanoparticle-decorated 3D cellulose nanofiber scaffolds *Carbohydrate Polymers* **273** 118603

[9] Silvestro I, Sergi R, D'Abusco A S, Mariano A, Martinelli A, Piozzi A and Francolini I 2021 Chitosan scaffolds with enhanced mechanical strength and elastic response by combination of freeze gelation, photo-crosslinking and freeze-drying *Carbohydrate Polymers* **267** 118156

[10] Li J, Sun H and Wang M 2020 Phase Inversion-Based Technique for Fabricating Bijels and Bijels-Derived Structures with Tunable Microstructures *Langmuir* **36** 14644-55

[11] Li H, Zheng L and Wang M 2021 Biofunctionalized Nanofibrous Bilayer Scaffolds for Enhancing Cell Adhesion, Proliferation and Osteogenesis *ACS Applied Bio Materials* **4** 5276-94

[12] Atala A 2020 Introduction: 3D Printing for Biomaterials *Chemical Reviews* **120** 10545-6

[13] Lai J, Wang C and Wang M 2021 3D printing in biomedical engineering: Processes, materials, and applications *Applied Physics Reviews* **8** 021322

[14] Wan T, Fan P, Zhang M, Shi K, Chen X, Yang H, Liu X, Xu W and Zhou Y 2022 Multiple Crosslinking Hyaluronic Acid Hydrogels with Improved Strength and 3D Printability *ACS Applied Bio Materials* **5** 334-43

[15] Gayer C, Ritter J, Bullemer M, Grom S, Jauer L, Meiners W, Pfister A, Reinauer F, Vučak M and Wissenbach K 2019 Development of a solvent-free polylactide/calcium carbonate composite for selective laser sintering of bone tissue engineering scaffolds *Mater. Sci. Eng. C* **101** 660-73

[16] Bose S, Bhattacharjee A, Banerjee D, Boccaccini A R and Bandyopadhyay A 2021 Influence of random and designed porosities on 3D printed tricalcium phosphate-bioactive glass scaffolds *Additive Manufacturing* **40** 101895

[17] Liang H, Wang Y, Chen S, Liu Y, Liu Z and Bai J 2022 Nano-Hydroxyapatite Bone Scaffolds with Different Porous Structures Processed by Digital Light Processing 3D Printing *Int J Bioprint* **8** 502-

[18] Gregor A, Filová E, Novák M, Kronek J, Chlup H, Buzgo M, Blahnová V, Lukášová V, Bartoš M, Nečas A and Hošek J 2017 Designing of PLA scaffolds for bone tissue replacement fabricated by ordinary commercial 3D printer *J. Biol. Eng.* **11** 31-

[19] Luo Y, Zhai D, Huan Z, Zhu H, Xia L, Chang J, Wu C J A a m and interfaces 2015 Three-dimensional printing of hollow-struts-packed bioceramic scaffolds for bone regeneration **7** 24377-83

[20] Trombetta R, Inzana J A, Schwarz E M, Kates S L and Awad H A 2017 3D Printing of Calcium Phosphate Ceramics for Bone Tissue Engineering and Drug Delivery *Annals of biomedical engineering* **45** 23

[21] Pires L S O, Fernandes M H F V and de Oliveira J M M 2018 Biofabrication of glass scaffolds by 3D printing for tissue engineering *Int. J. Adv. Manuf. Tech.* **98** 2665-76

[22] Sing S L, An J, Yeong W Y and Wiria F E 2016 Laser and electron‐beam powder‐bed additive manufacturing of metallic implants: A review on processes, materials and designs *J. Orthop. Res.* **34** 369-85

[23] Zhang W, Shi W, Wu S, Kuss M, Jiang X, Untrauer J B, Reid S P and Duan B 2020 3D printed composite scaffolds with dual small molecule delivery for mandibular bone regeneration *Biofabrication* **12** 035020

[24] Zhong L, Chen J, Ma Z, Feng H, Chen S, Cai H, Xue Y, Pei X, Wang J and Wan Q 2020 3D printing of metal–organic framework incorporated porous scaffolds to promote osteogenic differentiation and bone regeneration *Nanoscale* **12** 24437-49

[25] Jiang Y, Pan X, Yao M, Han L, Zhang X, Jia Z, Weng J, Chen W, Fang L, Wang X, Zhang Y, Duan R, Ren F, Wang K, Chen X and Lu X 2021 Bioinspired adhesive and tumor microenvironment responsive nanoMOFs assembled 3D-printed scaffold for anti-tumor therapy and bone regeneration *Nano Today* **39** 101182

[26] Holmes B, Zhu W, Li J, Lee J D and Zhang L G 2015 Development of novel three-dimensional printed scaffolds for osteochondral regeneration *Tissue Eng. Part A* **21** 403-15

[27] Kolesky D B, Truby R L, Gladman A S, Busbee T A, Homan K A and Lewis J A 2014 3D Bioprinting of Vascularized, Heterogeneous Cell‐Laden Tissue Constructs *Adv. Mater.* **26** 3124-30

[28] Li J, Wu C, Chu P K and Gelinsky M 2020 3D printing of hydrogels: Rational design strategies and emerging biomedical applications *Materials Science and Engineering: R: Reports* **140** 100543

[29] Ouyang L, Armstrong J P K, Chen Q, Lin Y and Stevens M M 2020 Void-Free 3D Bioprinting for In Situ Endothelialization and Microfluidic Perfusion *Advanced Functional Materials* **30** 1908349

[30] Ouyang L, Armstrong J P K, Lin Y, Wojciechowski J P, Lee-Reeves C, Hachim D, Zhou K, Burdick J A and Stevens M M 2020 Expanding and optimizing 3D bioprinting capabilities using complementary network bioinks *Science Advances* **6** eabc5529

[31] Kim B S, Jang J, Chae S, Gao G, Kong J-S, Ahn M and Cho D-W 2016 Three-dimensional bioprinting of cell-laden constructs with polycaprolactone protective layers for using various thermoplastic polymers *Biofabrication* **8** 035013

[32] Van Belleghem S, Torres Jr L, Santoro M, Mahadik B, Wolfand A, Kofinas P and Fisher J P 2020 Hybrid 3D Printing of Synthetic and Cell‐Laden Bioinks for Shape Retaining Soft Tissue Grafts *Advanced Functional Materials* **30** 1907145

[33] Wang C, Zhao Q and Wang M 2017 Cryogenic 3D printing for producing hierarchical porous and rhBMP-2-loaded Ca-P/PLLA nanocomposite scaffolds for bone tissue engineering *Biofabrication* **9** 025031

[34] Wang C, Ye X, Zhao Y, Bai L, He Z, Tong Q, Xie X, Zhu H, Cai D, Zhou Y, Lu B, Wei Y, Mei L, Xie D and Wang M 2020 Cryogenic 3D printing of porous scaffolds for in situ delivery of 2D black phosphorus nanosheets, doxorubicin hydrochloride and osteogenic peptide for treating tumor resection-induced bone defects *Biofabrication* **12** 035004

[35] Adamkiewicz M and Rubinsky B 2015 Cryogenic 3D printing for tissue engineering *Cryobiology* **71** 518-21

[36] Li H, Tan Y J, Liu S and Li L 2018 Three-Dimensional Bioprinting of Oppositely Charged Hydrogels with Super Strong Interface Bonding *ACS Applied Materials and Interfaces* **10** 11164-74

[37] Li H, Tan Y J, Kiran R, Tor S B and Zhou K 2021 Submerged and non-submerged 3D bioprinting approaches for the fabrication of complex structures with the hydrogel pair GelMA and alginate/methylcellulose *Additive Manufacturing* **37** 101640

[38] Duan B, Hockaday L A, Kang K H and Butcher J T 2013 3D Bioprinting of heterogeneous aortic valve conduits with alginate/gelatin hydrogels *Journal of Biomedical Materials Research Part A* **101** 1255-64

[39] Shapira A, Noor N, Asulin M and Dvir T 2018 Stabilization strategies in extrusion-based 3D bioprinting for tissue engineering *Applied Physics Reviews* **5** 041112

[40] Ouyang L 2022 Pushing the rheological and mechanical boundaries of extrusion-based 3D bioprinting *Trends Biotechnol*

[41] Markstedt K, Mantas A, Tournier I, Martínez Ávila H c, Hägg D and Gatenholm P 2015 3D bioprinting human chondrocytes with nanocellulose–alginate bioink for cartilage tissue engineering applications *Biomacromolecules* **16** 1489-96

[42] Ouyang L, Highley C B, Rodell C B, Sun W and Burdick J A 2016 3D printing of shear-thinning hyaluronic acid hydrogels with secondary cross-linking *ACS Biomaterials Science & Engineering* **2** 1743-51

[43] Li H, Tan Y J, Leong K F and Li L 2017 3D Bioprinting of Highly Thixotropic Alginate/Methylcellulose Hydrogel with Strong Interface Bonding *ACS applied materials & interfaces* **9** 20086

[44] Zhou F, Hong Y, Liang R, Zhang X, Liao Y, Jiang D, Zhang J, Sheng Z, Xie C, Peng Z, Zhuang X, Bunpetch V, Zou Y, Huang W, Zhang Q, Alakpa E V, Zhang S and Ouyang H 2020 Rapid printing of bio-inspired 3D tissue constructs for skin regeneration *Biomaterials* **258** 120287

[45] Wang X, Xu S, Zhou S, Xu W, Leary M, Choong P, Qian M, Brandt M and Xie Y M 2016 Topological design and additive manufacturing of porous metals for bone scaffolds and orthopaedic implants: a review *Biomaterials* **83** 127-41

[46] Ahn S, Lee H, Lee E J and Kim G 2014 A direct cell printing supplemented with low-temperature processing method for obtaining highly porous three-dimensional cell-laden scaffolds *Journal of Materials Chemistry B* **2** 2773-82

[47] Zhang M, Lin R, Wang X, Xue J, Deng C, Feng C, Zhuang H, Ma J, Qin C and Wan L 2020 3D printing of Haversian bone–mimicking scaffolds for multicellular delivery in bone regeneration *Science advances* **6** 6725

[48] Koons G L and Mikos A G 2019 Progress in three-dimensional printing with growth factors *Journal of controlled release* **295** 50-9

[49] Narayan R, Yoo J and Atala A 2021 3D bioprinting: Physical and chemical processes *Applied Physics Reviews* **8** 030401

[50] Wang C, Yue H, Huang W, Lin X, Xie X, He Z, He X, Liu S, Bai L, Lu B, Wei Y and Wang M 2020 Cryogenic 3D printing of heterogeneous scaffolds with gradient mechanical strengths and spatial delivery of osteogenic peptide/TGF-β1 for osteochondral tissue regeneration *Biofabrication* **12** 025030

[51] Li S, Xu Y, Yu J and Becker M L 2017 Enhanced osteogenic activity of poly(ester urea) scaffolds using facile post-3D printing peptide functionalization strategies *Biomaterials* **141** 176-87

[52] Trino L D, Bronze-Uhle E S, Ramachandran A, Lisboa-Filho P N, Mathew M T and George A 2018 Titanium surface bio-functionalization using osteogenic peptides: Surface chemistry, biocompatibility, corrosion and tribocorrosion aspects *Journal of the Mechanical Behavior of Biomedical Materials* **81** 26-38

[53] Yan Y, Chen H, Zhang H, Guo C, Yang K, Chen K, Cheng R, Qian N, Sandler N and Zhang Y S 2019 Vascularized 3D printed scaffolds for promoting bone regeneration *Biomaterials* **190** 97-110

[54] Wang C, Huang W, Zhou Y, He L, He Z, Chen Z, He X, Tian S, Liao J, Lu B, Wei Y and Wang M 2020 3D printing of bone tissue engineering scaffolds *Bioact. Mater.* **5** 82-91

LIST OF FIGURES

Figure 7 Comparison of cell distribution onto the two-layer GGOTP scaffolds prepared via (1) post cell seeding and (2) *in situ* cell loading (i.e., cell printing). (a) Schematic illustration of these two strategies; (b) fluorescence images representing the cell viability, cell density and cell distribution onto the scaffolds after *in vitro* culture at day 3 and day 7; (c) histogram of cell area fraction; (d) histogram of cell distribution index.

Figure 8 Osteogenic differentiation of rBMSCs in GGTP and GGOTP scaffolds. (a, b) ALP staining (blue area) of rBMSCs for the (a) GGTP scaffolds and (b) GGOTP scaffolds after 14-day *in vitro* culture; (c, d) ARS staining of rBMSCs (released from the GG rods and then precipitated onto the substrate of the culture dish) for the (c) GGTP scaffolds and (d) GGOTP scaffolds after 21-day *in vitro* culture; (e) ALP activity of rBMSCs for GGTP and GGOTP scaffolds for up to 14 days; (f) quantitative analysis of the dissolved calcium nodules after 21-day *in vitro* culture (Scale bar: 100 μm).